PHYSICAL REVIEW LETTERS

Chimera States in Populations of Nonlocally Coupled Chemical Oscillators

Simbarashe Nkomo, Mark R. Tinsley, and Kenneth Showalter

C. Eugene Bennett Department of Chemistry, West Virginia University, Morgantown, West Virginia 26506-6045, USA
(Received 1 February 2013; published 14 June 2013)

Chimera states occur spontaneously in populations of coupled photosensitive chemical oscillators. Experiments and simulations are carried out on nonlocally coupled oscillators, with the coupling strength decreasing exponentially with distance. Chimera states with synchronized oscillators, phase waves, and phase clusters coexisting with unsynchronized oscillators are analyzed. Irregular motion of the cores of asynchronous oscillators is found in spiral-wave chimeras.

Common coupling schemes for describing interacting oscillators include global coupling, where each oscillator is coupled equally to all other oscillators, and local coupling, where each oscillator is coupled only to its nearest neighbors [1]. Nonlocal coupling schemes, where each oscillator is coupled to a range of nearby oscillators, lie between the extremes of global and local coupling [2–9]. The coupling strength in nonlocal coupling typically attenuates with decreasing oscillator proximity, although it can take on a variety of forms. Nonlocal coupling is found in natural and synthetic systems, for example, neuronal networks and arrays of Josephson junctions [4,10,11].

In early studies of nonlocal coupling, Kuramoto and co-workers [2,3] found highly unusual synchronization dynamics, later called the chimera state [4], which consisted of coexisting subpopulations of synchronized and unsynchronized oscillators, even though the oscillators were identical and were coupled to each other in an identical manner. They studied 1D and 2D systems of oscillators in ring [2] and planar [3] configurations, with the coupling strength decreasing exponentially with distance. In the 2D case, the partitioning of synchronized and unsynchronized oscillators takes the form of a spiral wave rotating around a region of unsynchronized oscillators.

Chimera states have recently been studied experimentally by Hagerstrom *et al.* [12] in coupled-map lattices and by Tinsley *et al.* [13] in populations of chemical oscillators. The coupled-map lattice experiments [12] were based on a camera-spatial light modulator (SLM) system, with each oscillator coupled to a range of neighboring oscillators [9]. The chemical oscillator experiments [13] were based on coupling photosensitive oscillators with a camera-SLM system and utilized two coupling strengths, following the scheme of Abrams *et al.* [7].

In this Letter, we report on experimental and computational studies of coupled photosensitive chemical oscillators. We follow a Kuramoto-like nonlocal coupling scheme [2,3], with the nearest neighbors having the strongest coupling and the coupling strength for each successive neighbor falling off exponentially. We report new aspects of chimera behavior, including groups of unsynchronized

oscillators serving as the source of synchronized 1D phase waves. Meandering synchronized groups of oscillators in 1D experiments and simulations provide insights into the meandering asynchronous spiral cores found in 2D simulations with a realistic model of the coupled chemical oscillators.

Experiments are carried out with the Belousov-Zhabotinky (BZ) reaction [14], where catalyst particles in catalyst-free reaction mixtures form populations of discrete chemical oscillators [13,15]. The BZ reaction is photosensitive with the $Ru(bipy)_3^{2+}$ catalyst [16], which, when loaded onto cation-exchange particles, allows manipulation of the phase of each oscillator with light from an SLM. The gray level I_j of each oscillator is monitored with a CCD camera, which is then used to calculate the appropriate light perturbation ϕ_j from the SLM according to the coupling relation

$$\phi_j = \phi_0 + \sum_{\rho=j-n}^{j+n} K(I_\rho(t-\tau) - I_j(t)), \qquad (1)$$

where ϕ_0 is the background light intensity [17], τ is a time delay [6] in the feedback from neighboring oscillator ρ to oscillator j, and $j = 1, 2, \ldots, N$. The coupling radius is n (number of coupled neighbors on each side of oscillator j), and the coupling function is given by $K = K' \exp(-\kappa|\rho - j|)$, where K' and κ are constants that govern the effective coupling strength and range of each oscillator.

The experiments are carried out with 40 oscillators in a ring configuration, coupled according to Eq. (1). Figure 1 shows an example of typical experimental behavior, where a snapshot of the phase of each oscillator at $t = 1220$ s is shown in Fig. 1(a). We see a group of synchronized oscillators with oscillator index $j = 9$–17 and unsynchronized oscillators with $j = 1$–8 and $j = 30$–40. Oscillators with $j = 18$–29 form a diagonal feature, which represents a splay-like state [18].

Figure 1(b) shows the phase calculated from the measured gray level as a function of time for each of the oscillators. The spontaneous appearance of the group of synchronized oscillators can be seen at $t \approx 300$ s.
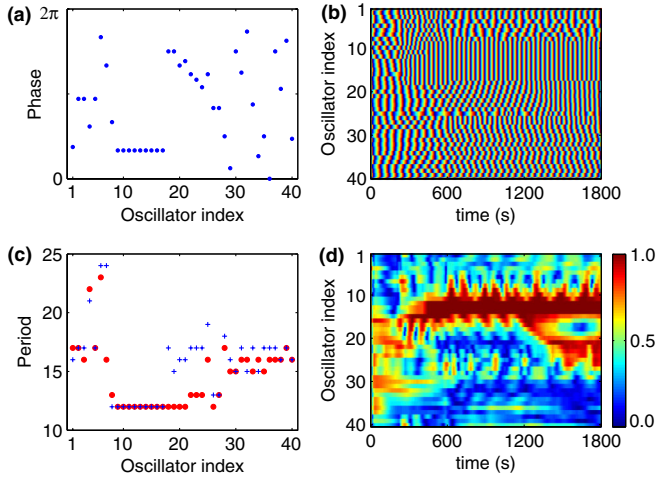
FIG. 1 (color online).   Experimental behavior of 40 oscillators coupled according to Eq. (1) in a ring configuration, with $n = 10$, $\kappa = 0.5$, $K' = 1$, and $\tau = 30$ s. The experiment was started with a quasirandom initial phase distribution of the oscillators. (a) Snapshot showing the phase of each oscillator at $t = 1220$ s. (b) Phase of each oscillator as a function of time. (c) Period of each oscillator at $t = 900$ s (blue +) and 1500 s (red bullet). (d) Local order parameter R according to Eq. (2) as a function of time, with $m = 3$. See the Supplemental Material [25] for a video of the phase of each oscillator in (a) as a function of time.

The diagonal wave feature occurs at $t \approx 600$–1200 s, and, at $t \approx 1200$–1400 s, it transforms into a group of synchronized oscillators that are out of phase with the original synchronized group. Figure 1(c) shows the period of each oscillator for two different times, demonstrating that the simultaneous firing of the synchronized oscillators gives rise to a shorter oscillatory period than that of the unsynchronized oscillators.

The evolution of the chimera state in terms of the local order parameter R [9], defined by

$$R(j, t) = \frac{1}{2m} \left| \sum_{\rho = j-m}^{j+m} \exp[i\theta(\rho, t)] \right|, \quad (2)$$

is shown in Fig. 1(d), where $j = 1, 2, \dots, N$, and m is the sampling radius. The high order of the original group of synchronized oscillators can be seen as well as the region of synchronization appearing at $t \approx 1400$ s. The remaining unsynchronized oscillators make up the surrounding regions of low order. Size oscillations of the synchronized group occur as the higher-frequency oscillators "lap" the unsynchronized oscillators, and neighboring oscillators transiently join the synchronized group when their phases align.

Many nonlocal coupling experiments were carried out, some with quasirandom distributions of the initial phases and others with special initial conditions. In the first case, a group of synchronized oscillators typically appeared spontaneously, with different realizations usually giving

rise to different regions of synchronized and unsynchronized oscillators. In experiments with special initial conditions, a group of synchronized oscillators approximately the size of a spontaneously formed group was produced by using perturbations in illumination intensity, while the remaining oscillators had a quasirandom distribution of phases. In these experiments, the region of synchronization typically evolved in time, either disappearing with another synchronized region appearing or shifting to another region among the unsynchronized oscillators. The photosensitive chemical oscillators have an inherent distribution in the oscillatory period (60.0 ± 4.0 s) that arises from the size distribution of the catalytic particles. The oscillator populations with this distribution allowed full synchronization of the oscillators in addition to the chimera state for the same conditions, ensuring that a partially entrained state with synchronized and unsynchronized oscillators arising from an overly broad frequency distribution did not occur [7,19].

Simulations of the nonlocally coupled chemical oscillators were carried out using the two-variable Zhabotinsky-Buchholtz-Kiyatkin-Epstein (ZBKE) model for the BZ reaction [20], modified to describe the photosensitivity of the Ru(bpy)$^{2+}$ catalyzed discrete oscillator system [21]: $dX_j/dt = f(X_j, Z_j, q_j) + \phi_j/\epsilon_1$, $dZ_j/dt = g(X_j, Z_j, q_j) + 2\phi_j$, where f and g represent the nonphotochemical components of the BZ reaction, and X_j, Z_j, and q_j are [HBrO$_2$], [Ru(bpy)$^{3+}$], and the stoichiometric factor associated with the jth oscillator. A Gaussian distribution in oscillatory period, reflecting the experimental period distribution, was realized by using a Gaussian distribution in the value of q_j. The photoexcitatory feedback on oscillator j is ϕ_j, calculated according to Eq. (1), where the gray levels I_ρ and I_j are replaced by the catalyst concentrations Z_ρ and Z_j.

Figure 2 shows behavior from a simulation of the nonlocally coupled BZ oscillator system, where a group of oscillators spontaneously synchronized at $t \approx 2.0 \times 10^3$ to form a chimera state of synchronized and unsynchronized oscillators. Figure 2(a) shows a snapshot of the phase of each oscillator at $t = 1.90 \times 10^4$. The phase of each oscillator as a function of time in Fig. 2(b) illustrates the stability of the synchronized group but also illustrates the complex behavior of the unsynchronized oscillators, which tend to form transient diagonal wave features as well as transient in-phase or out-of-phase synchronization of a few oscillators. Figure 2(c) shows that the period of the synchronized oscillators is significantly shorter than that of the unsynchronized oscillators, much like the experimental system shown in Fig. 1(c). Figure 2(d) illustrates the evolution of the chimera state according to the local order parameter R in Eq. (2). We again see features that correspond to size variations of the synchronized group, although in this example the changes are irregular.

Several different types of chimera behavior were found in our experiments and simulations, for example, the
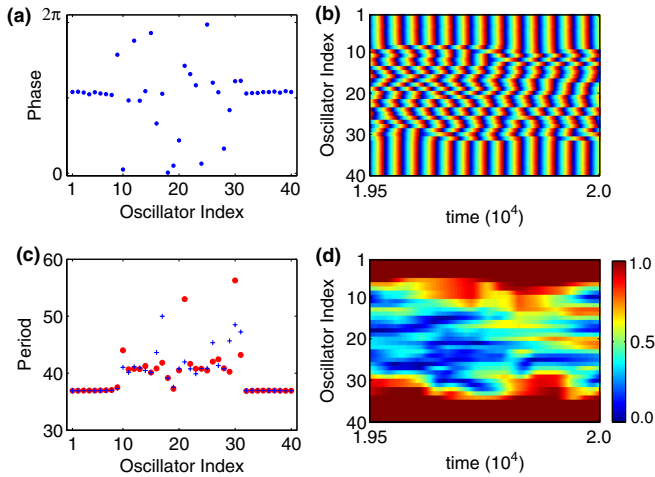
FIG. 2 (color online). Model simulations of 40 coupled BZ oscillators in a ring configuration, with $n = 10$, $\kappa = 0.4$, $K' = 6.3 \times 10^{-5}$, $\tau = 35.0$, and $\phi_0 = 1.6 \times 10^{-4}$. The simulation was started with a random initial phase distribution. (a) Snapshot showing the phase of each oscillator at $t = 1.90 \times 10^4$. (b) Phase of each oscillator as a function of time. (c) Period of each oscillator at $t = 1.85 \times 10^4$ (blue +), 1.90×10^4 (red bullet). (d) Local order parameter R as a function of time, with $m = 3$. See the Supplemental Material [25] for a video of the phase of each oscillator in (a) as a function of time.

coexistence of unsynchronized oscillators with synchronized phase waves, as shown in Fig. 3(a). Video images show that the waves are initiated from a small region of unsynchronized oscillators, with oscillator index $j = 30$–34. On the right-hand side, the wave travels along the diagonal $j = 35$–40, where it continues through the periodic boundary to $j = 1$–9. The wave on the left-hand side $j = 24$–29 travels to a group of unsynchronized oscillators $j = 10$–23 corresponding to the collision region of the two waves. The phase of each oscillator as a function of time shows the persistence of the wave features; see Fig. 3(b). This phase-wave behavior is likely related to q-twisted states described in theoretical studies [18]. Complex behavior is again seen in the unsynchronized oscillators, with small groups becoming transiently synchronized in wavelike structures.

In addition to chimera states with synchronized wave behavior, we also find phase-cluster chimera states [6], where two or more out-of-phase groups of synchronized oscillators coexist with unsynchronized oscillators. Figure 3(c) shows a snapshot of the phase of each oscillator in an experimental phase-cluster chimera at $t = 1206$ s. We see two clusters of synchronized oscillators having the same phase with $j = 5$–10 and $j = 22$–29 and a third out-of-phase cluster with $j = 33$–37. The local order parameter R as a function of time in Fig. 3(d) shows that these clusters persist and, interestingly, that the first cluster displays prominent antiphase size oscillations.

Simulations based on the photosensitive BZ oscillator model have also been carried out in a planar two-dimensional
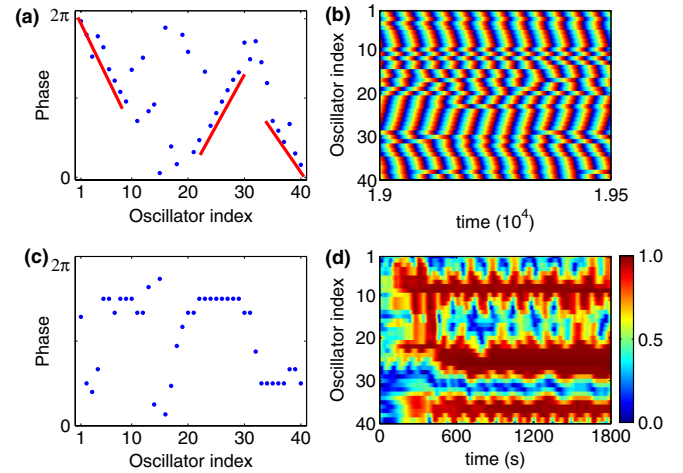

FIG. 3 (color online). Simulations of phase-wave chimera states (top) and experimental measurements of phase-cluster chimera states (bottom). (a) Model simulations of 40 coupled BZ oscillators, with $n = 10$, $\kappa = 0.4$, $K' = 6.3 \times 10^{-5}$, $\tau = 35.0$, and $\phi_0 = 1.6 \times 10^{-4}$. The snapshot shows the phase of each oscillator at $t = 1.93 \times 10^4$, where the red lines have been added to guide the eye. The simulation was started with a random initial phase distribution. (b) Phase of each oscillator in (a) as a function of time. (c) Measurements showing experimental phase-cluster chimera in 40 coupled BZ oscillators, with $n = 10$, $\kappa = 0.8$, $K' = 1.0$, and $\tau = 30.0$ s. The experiment was started with a quasirandom initial phase distribution; the snapshot shows the phase of each oscillator at $t = 1206$ s. (d) Local order parameter R of oscillators in (c) as a function of time, with $m = 3$. See the Supplemental Material [25] for videos of the phase of each oscillator in (a) and (c) as a function of time.

configuration. We use the same nonlocal coupling, with the separation of the oscillators determined by the Pythagorean distance according to the oscillator indices in the square lattice, which is typically made up of 50×50 oscillators [22]. The spiral cores of asynchronous oscillators meander in an irregular manner, with the form of the meandering sensitive to the value of the delay τ. Figures 4(a) and 4(b) show snapshots of pairs of initially symmetrical counterrotating spirals at $t = 3500$ for two slightly different values of τ. A 2D local order parameter can be calculated through generalization of Eq. (2), and the value of R at each point in Figs. 4(a) and 4(b) is shown in Figs. 4(c) and 4(d). The meander of the asynchronous core is tracked by following the minimum in R, and Fig. 4(c) illustrates the case in which the asynchronous cores undergo approximately random-walk behavior. We have observed cases in which the mean-squared displacement is linear with time, although we also find deviations from this behavior. Figure 4(d) shows larger irregular motions of the cores of asynchronous oscillators. The irregular motion in both cases is similar to that of reaction-diffusion spiral cores in the presence of spatiotemporal noise imposed on the medium excitability [23].
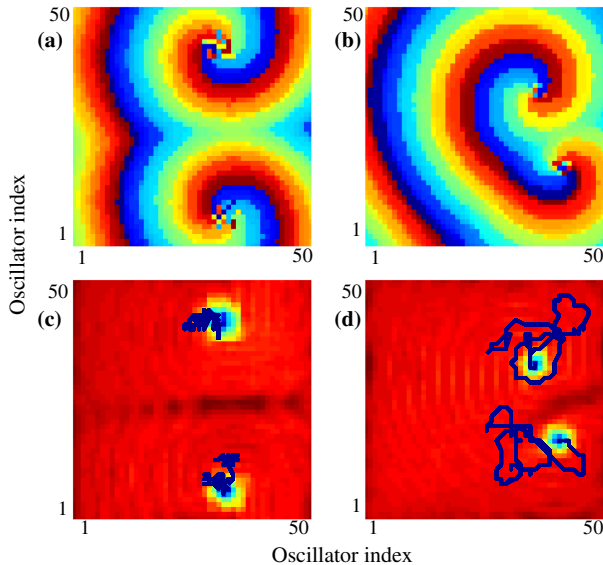
FIG. 4 (color online). Simulations of spiral chimera states in populations of BZ oscillators. The system is composed of 50×50 oscillators in a square-lattice configuration, with a coupling radius of $n = 4$ and fixed boundary conditions. The top images show the phase of each oscillator in the lattice at $t = 3500$ for values of delay $\tau = 4.0$ (a) and 3.4 (b). Each simulation is initiated with a pair of symmetric counterrotating spirals, with $\tau = 0$. The delay is switched on at $t = 500$, and the simulation is continued to $t = 3500$. (c), (d) Shown is the local order parameter R at $t = 3500$. The dark blue line shows the trajectory of the minimum in R between $t = 700$ and 3500. Parameters: $\kappa = 0.3$, $K' = 1.4 \times 10^{-3}$, and $\phi_0 = 1.1 \times 10^{-4}$. See the Supplemental Material [25] for videos of the evolution of each spiral pair in (a), (b) and the spiral-core trajectory as a function of time in (c), (d).

The irregular meandering behavior arises from the interaction of the core of asynchronous oscillators with the spiral-wave tip. As the tip rotates, it experiences different asynchronous oscillators, which, depending on the oscillator phase, cause the tip to grow or contract. The interaction may occur with more than the outer "boundary" of asynchronous oscillators when transient phase alignment occurs with the interior oscillators, leading to larger fluctuations of the spiral tip. Changes in the spiral tip also lead to distortions of the shape of the core of asynchronous oscillators. Similar complex motion of spiral centers has been reported in two-dimensional systems of coupled phase-shifted oscillators, with the rigid rotating solution typically becoming unstable with increasing phase shift [24].

Our experiments and modeling studies of chimera behavior in 1D ring configurations provide insights into spiral chimera behavior in 2D. In both the 1D phase-wave chimera [Fig. 3(a)] and the 2D spiral-wave chimera (Fig. 4), the waves originate from a group of unsynchronized oscillators. The 1D out-of-phase wave initiation shown in Fig. 3(a) is suggestive of a 1D spiral wave and

is related to q-twisted states [18]. The size variations of the groups of synchronized oscillators seen in 1D [Figs. 1(d), 2(d), and 3(d)] are related to the meandering behavior of the spiral core of asynchronous oscillators in 2D.

Note added in proof.—A new experimental example of chimera states has been studied in mechanical oscillator networks [26].

[1] Y. Kuramoto, *Chemical Oscillations, Waves, and Turbulence* (Springer, New York, 1984); A. Pikovsky, M. Rosenblum, and J. Kurths, *Synchronization: A Universal Concept in Nonlinear Sciences* (Cambridge University Press, Cambridge, England, 2003).
[2] Y. Kuramoto and D. Battogtokh, Nonlinear Phenom. Complex Syst. **5**, 380 (2002).
[3] S. I. Shima and Y. Kuramoto, Phys. Rev. E **69**, 036213 (2004).
[4] D. M. Abrams and S. H. Strogatz, Phys. Rev. Lett. **93**, 174102 (2004).
[5] D. M. Abrams and S. H. Strogatz, Int. J. Bifurcation Chaos Appl. Sci. Eng. **16**, 21 (2006).
[6] G. C. Sethia, A. Sen, and F. M. Atay, Phys. Rev. Lett. **100**, 144102 (2008).
[7] D. M. Abrams, R. Mirollo, S. H. Strogatz, and D. A. Wiley, Phys. Rev. Lett. **101**, 084103 (2008).
[8] A. E. Motter, Nat. Phys. **6**, 164 (2010).
[9] I. Omelchenko, Y. Maistrenko, P. Hovel, and E. Schöll, Phys. Rev. Lett. **106**, 234102 (2011).
[10] J. D. Murray, *Mathematical Biology* (Springer, New York, 1989).
[11] J. R. Phillips, H. S. J. van der Zant, J. White, and T. P. Orlando, Phys. Rev. B **47**, 5219 (1993).
[12] A. M. Hagerstrom, T. E. Murphy, R. Roy, P. Hovel, I. Omelchenko, and E. Schöll, Nat. Phys. **8**, 658 (2012).
[13] M. R. Tinsley, S. Nkomo, and K. Showalter, Nat. Phys. **8**, 662 (2012).
[14] A. N. Zaikin and A. M. Zhabotinsky, Nature (London) **225**, 535 (1970).
[15] A. F. Taylor, P. Kapetanopoulos, B. J. Whitaker, R. Toth, L. Bull, and M. R. Tinsley, Phys. Rev. Lett. **100**, 214101 (2008).
[16] L. Kuhnert, Nature (London) **319**, 393 (1986).
[17] The intensity I_j of each oscillator is measured in gray level, and the projected light intensity ϕ_j is determined by the gray level, where the background intensity $\phi_0 = 140$, which is equal to 1.4 mW cm^{-2}.
[18] T. Girnyk, M. Hasler, and Y. Maistrenko, Chaos **22**, 013114 (2012).
[19] A. T. Winfree, J. Theor. Biol. **16**, 15 (1967).
[20] A. M. Zhabotinsky, F. Buchholtz, A. B. Kiyatkin, and I. R. Epstein, J. Phys. Chem. **97**, 7578 (1993).
[21] Simulations were carried out with the two-variable ZBKE model [20] modified to describe the photosensitive discrete BZ oscillator system [13,15], where
$\epsilon_1(dX_j/dt) = \phi_j - X_j^2 - X_j + \epsilon_2 \gamma u_{ss}^2 + u_{ss}(1 - Z_j) + [(\mu - X_j)/(\mu + X_j)][q\alpha Z_j/(\epsilon_3 + 1 - Z_j) + \beta]$ and

$dZ_j/dt = 2\phi_j + u_{ss}(1 - Z_j) - [\alpha Z_j/(\epsilon_3 + 1 - Z_j)]$ describes the chemistry of oscillator j. The variables X_j and Z_j and the constant q_j represent [HBrO$_2$], tris(2, 2'-bipyridine)ruthenium(3+) ion [Ru(bpy)$_3^{3+}$], and the stoichiometric coefficient, respectively, associated with oscillator j. The photoexcitatory feedback associated with oscillator j is ϕ_j. Nondimensional model parameters are $\epsilon_1 = 0.11$, $\epsilon_2 = 1.7 \times 10^{-5}$, $\epsilon_3 = 1.6 \times 10^{-3}$, $\gamma = 1.2$, $\alpha = 0.10$, $\beta = 1.7 \times 10^{-5}$, $\mu = 2.4 \times 10^{-4}$, and a distribution in q that gives a period of 41.0 ± 2.1.

[22] Each oscillator j is mapped onto a 2D grid, where $l \times l = 50 \times 50$, with integer lattice coordinates (p, q) such that $j = p + l(q - 1)$. The Pythagorean distance between two oscillators j and j' is given by $[(p - p')^2 + (q - q')^2]^{1/2}$.

[23] I. Sendiña-Nadal, S. Alonso, V. Pérez-Muñuzuri, M. Gómez-Gesteira, V. Pérez-Villar, L. Ramírez-Piscina, J. Casademunt, J. M. Sancho, and F. Sagués, Phys. Rev. Lett. **84**, 2734 (2000).

[24] J. Paullet and G. Ermentrout, SIAM J. Appl. Math. **54**, 1720 (1994); P.-J. Kim, T.-W. Ko, H. Jeong, and H.-T. Moon, Phys. Rev. E **70**, 065201 (2004); E. A. Martens, C. R. Laing, and S. H. Strogatz, Phys. Rev. Lett. **104**, 044101 (2010).

[25] See Supplemental Material at http://link.aps.org/supplemental/10.1103/PhysRevLett.110.244102 for experimental setup and videos associated with Figs. 1–4.

[26] E. A. Martens, S. Thutupalli, A. Fourrière, and O. Hallatschek, arXiv:1301.7608 [Proc. Natl. Acad. Sci. U.S.A. (to be published)].